CHAPTER ELEVEN

Synthetic cell-like membrane interfaces for probing dynamic protein-lipid interactions

Spencer T. Glantz[†], **Erin E. Berlew**[†], **Brian Y. Chow***
Department of Bioengineering, University of Pennsylvania, Philadelphia, PA, United States
*Corresponding author: e-mail address: bchow@seas.upenn.edu

Contents

Abstract

The ability to rapidly screen interactions between proteins and membrane-like interfaces would aid in establishing the structure-function of protein-lipid interactions, provide a platform for engineering lipid-interacting protein tools, and potentially inform the signaling mechanisms and dynamics of membrane-associated proteins.

[†] Authors contributed equally.

Methods in Enzymology, Volume 622
ISSN 0076-6879
https://doi.org/10.1016/bs.mie.2019.02.015

Here, we describe the preparation and application of water-in-oil (w/o) emulsions with lipid-stabilized droplet interfaces that emulate the plasma membrane inner leaflet with tunable composition. Fluorescently labeled proteins are easily visualized in these synthetic cell-like droplets on an automated inverted fluorescence microscope, thus allowing for both rapid screening of relative binding and spatiotemporally resolved analyses of for example, protein-interface association and dissociation dynamics and competitive interactions, using commonplace instrumentation. We provide protocols for droplet formation, automated imaging assays and analysis, and the production of the positive control protein BcLOV4, a natural photoreceptor with a directly light-regulated interaction with anionic membrane phospholipids that is useful for optogenetic membrane recruitment.

1. Introduction

1.1 Overview

Many key cellular signaling processes in environmental sensing, development, and migration are mediated by dynamic protein-lipid interactions with the plasma membrane, including the recruitment to and undocking from the inner leaflet. The ability to rapidly probe the lipid interactions of these membrane-associated proteins in a highly controlled manner on commoditized instrumentation would facilitate structure-function analyses, inform their signaling mechanism and dynamics, and provide an assay platform for engineering lipid-interacting protein tools.

Protein-lipid overlay (PLO) assays are a common high throughput methodology for screening protein-lipid interactions (Dowler et al., 2000; Gallego et al., 2010; Kavran et al., 1998; Park et al., 2007), but these assays test for headgroup interactions without recapitulating a membrane interface and are prone to false positives (Narayan & Lemmon, 2006; Yu et al., 2004). Another protein-lipid binding assay that can be performed without complex instrumentation is the liposome pulldown (Lee et al., 2002; Pykäläinen et al., 2011; Tay, Wang, & Du, 2017). Yet, this assay requires the isolation of lipid-bound protein by ultra-centrifugation or solid-support immobilization of protein (Lu et al., 2012; Zhu et al., 2001), making it challenging to study proteins that are unstable in aqueous solution and liable to precipitate (as many lipid-interacting proteins are). Additionally, the assay is low-throughput because results must be resolved in gels. Gold-standard techniques for determining protein affinity are often inaccessible or poorly suited for widescale screening due to cost, such as surface plasmon resonance (SPR)

(Beseničar, Maček, Lakey, & Anderluh, 2006; Tang, Zeng, & Liang, 2010), or due to large milliliter-scale protein volumes, such as isothermal titration calorimetry (ITC) (Seelig, 2004).

Fluorescence imaging of water-in-oil (w/o) emulsions with lipid-stabilized droplet interfaces offers a complementary platform for screening protein-lipid interactions, determining relative affinities, and monitoring interaction dynamics (Glantz et al., 2018). In this system, the droplet interior emulates the cytosol, while the lipid monolayer-stabilized droplet interface emulates the plasma membrane inner leaflet (Fig. 1). Lipid interfaces are simple to produce as single-emulsions by brief agitation of lipid-containing decane oil (the continuous phase of the emulsion) and a much lower volume of protein-containing aqueous solution (the dispersed phase of the emulsion). Single-emulsions (typically, without lipid-stabilization) have long been used prevalently in clonal library preparation in next-generation sequencing (Head et al., 2014; Liu et al., 2012) and emulsion and digital droplet PCR (Pinheiro et al., 2012; Shao et al., 2011). However, they have also been adapted as synthetic cell-like structures for cell-free in vitro compartmentalization for directed evolution (Lu & Ellington, 2013; Tawfik & Griffiths, 1998) and for size tuning in exploring the role of cytoplasmic volume in development (Good, 2016; Good, Vahey, Skandarajah, Fletcher, & Heald, 2013).

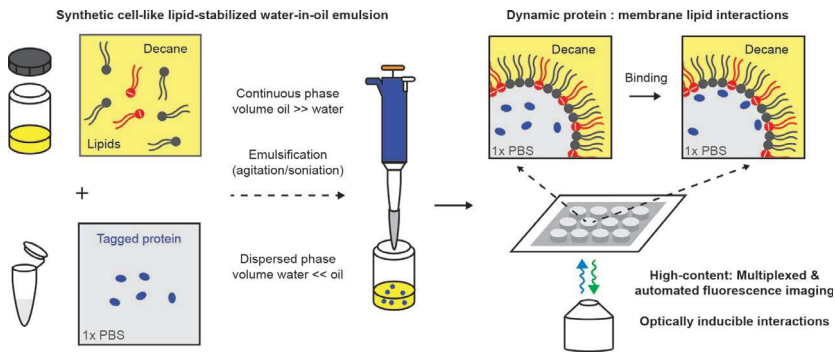

Fig. 1 Probing dynamic interactions between proteins and membranes in synthetic cell-like lipid-stabilized water-in-oil (w/o) emulsions. Preparation of (10^{-5} m-sized) synthetic cell-like droplets by emulsification, where the dispersed aqueous phase emulates the cell cytosol, and the lipid-stabilized water/oil interface emulates the plasma membrane inner leaflet. Protein:membrane lipid interactions can be screened by automated fluorescence imaging in synthetic cell-like droplets in vitro. Quantitative analysis of spatiotemporal interaction dynamics is facilitated by optical induction with purified recombinant optogenetic tools or photochemical uncaging.

Several aspects of lipid-stabilized single-emulsions make them simple to implement for protein-lipid screening applications and in-depth analyses alike. The composition of the interface is easily tuned by adjusting the lipid mixture in the oil phase prior to emulsification, which only requires pipetting or bath sonication to recapitulate the membrane-like structure. Only a small amount of protein is required per experiment (~1 μL per assay), which is helpful considering that lipid-interacting proteins are often challenging to solubilize. Once formed, the relative lipid-binding of fluorescently labeled proteins is imaged using an inverted epi-fluorescence microscope, one of the most common instruments found in any biomedical laboratory.

The microscopy-based analysis is amenable to automation and customization in medium-throughput assays in multi-well plate format, and temporally precise induction using light-responsive proteins (Glantz et al., 2018) or photocaged ligands (Caldwell et al., 2018). Recently, we used this platform to establish the relative lipid-binding selectivity and signaling structure-function of BcLOV4, a natural photosensory protein that binds anionic membrane phospholipids through a directly light-regulated electrostatic interaction (Glantz et al., 2018); when expressed in cells, this protein is also useful as a single-component system for optogenetic membrane recruitment of fused proteins. In this report, we show further examples of spatiotemporally resolved and quantitative analyses that can performed using the w/o emulsion platform, such as determining membrane association and undocking/dissociation kinetics of BcLOV4 and estimating its diffusional sampling distance (see Section 1.2).

Here, we provide protocols for droplet formation and automated fluorescence imaging and analysis in MATLAB (including code). We also report the production of BcLOV4 protein, which is particularly suitable as a control because it binds a wide range of anionic lipids when optically induced with easily delivered levels of blue light (Glantz et al., 2018). Ultimately, the synthetic cell-like membrane system is useful for (i) screening natural or engineered protein variants to gain structural design insights into lipid-binding function, (ii) testing the specificity of a lipid-binding protein for various lipid compositions, (iii) identifying membrane interactions without the confounding presence of other proteins in cells, and (iv) studying spatiotemporal dynamics of protein-membrane interactions through time-resolved imaging aided by conditional activation by optochemical and optogenetic tools.

1.2 Example quantitative and dynamic analyses

Time-resolved and high-content analysis of single cells is one of the most important uses of fluorescence microscopy. As described here, protein-membrane dynamics in synthetic cell-like structures can mirror and/or inform cellular protein-lipid interactions. For example, the post-illumination membrane association kinetics of our BcLOV4 control protein, and its membrane dissociation/undocking kinetics in the dark, are similar in this in vitro system to the timescales observed in eukaryotic cells (Fig. 2).

More spatiotemporally complex biophysical insights can be inferred in this cell free-system, such as the diffusional sampling distance (Lauffenburger & Linderman, 1993) of membrane-interacting proteins (Fig. 3). In the absence of an anionic membrane target or electrostatic stabilization, activated BcLOV4 in bulk solution in vitro will form large colloidal aggregates (>1 μm in size). In large droplets, the two simultaneous processes, of high-affinity membrane binding and the less preferred self-aggregation, result in a dark halo between the droplet interface and an interior core of observable colloids (Fig. 3A-C). The size of this region of depleted protein is indicative of the sampling distance over which the protein can encounter its high-affinity membrane sink, whereas beyond this distance from an anionic membrane (or in the absence of one), the protein self-aggregates (Fig. 3D-G). Photoactivated BcLOV4 has an observed sampling distance of ~12 μm regardless of droplet size, which is larger than the typical eukaryotic cell radius, thus informing why colloidal BcLOV4 photobodies are not formed in the cytosol of cells.

2. Generation of phospholipid-stabilized emulsion droplets

The method reported here for creating synthetic cell-like emulsion droplets (Fig. 4) is adapted from work by others in cell-free signaling (Caldwell et al., 2018; Good, 2016; Good et al., 2013). We first solubilize the lipids in chloroform to facilitate dispensing, and then the organic solvent is evaporated to generate a lipid film that is subsequently resuspended in decane oil and blended with other lipids to the desired relative composition. Separately, fluorescently labeled protein is prepared in aqueous buffer. Vigorous mixing of the aqueous and decane solutions results in a uniform emulsion, where the aqueous solution is the droplet interior or emulsion dispersed phase when its volume is much lower than the oil volume, which will be the droplet exterior or continuous phase.

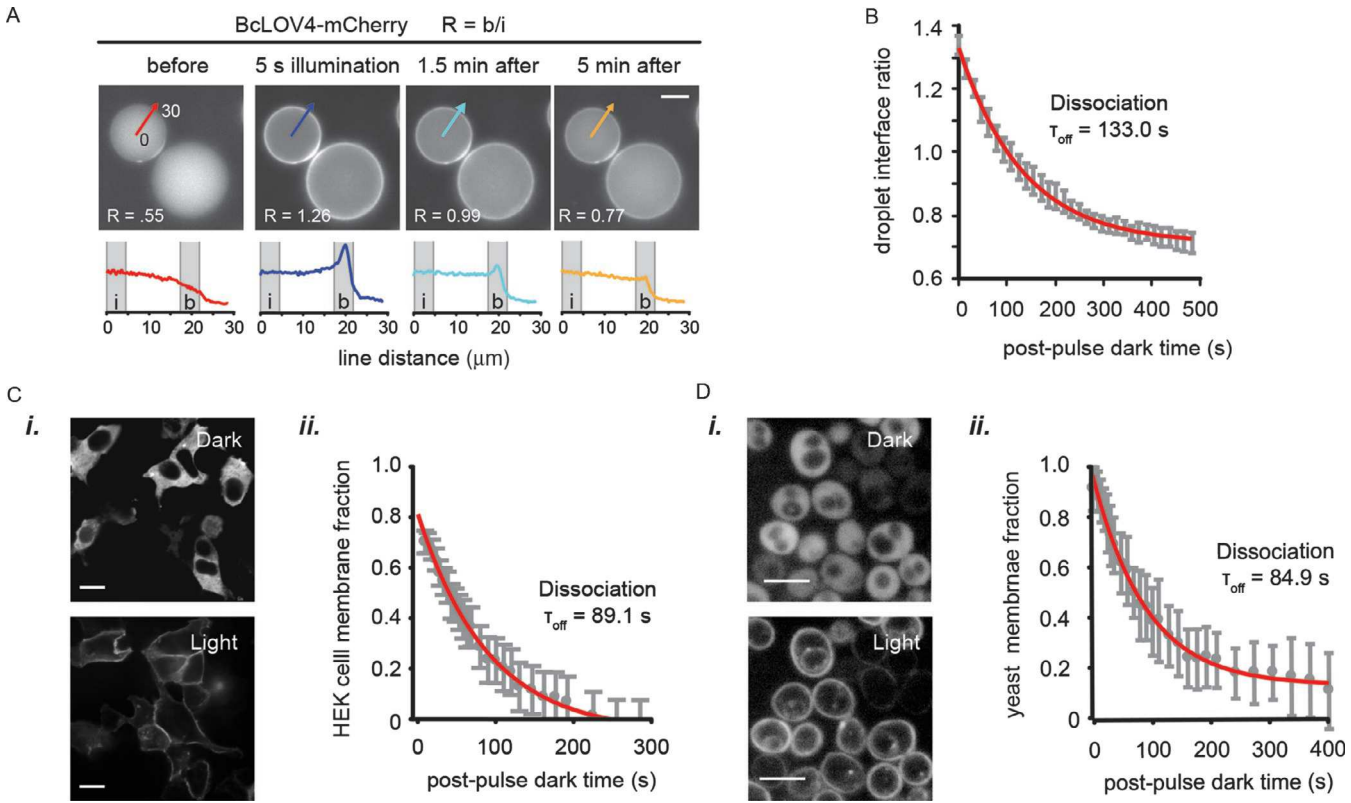

Fig. 2 See legend on opposite page.

Note 2.1. This protocol describes the generation of phospholipid-stabilized water-in-oil emulsion droplets that have a lipid composition of 80% phosphatidylcholine (PC) and 20% phosphatidylserine (PS), but these lipids may be substituted for alternative lipids.

Note 2.2. Qualitative interaction screening is possible with phosphatidylinositol phosphates (PIPs), based on our results with BcLOV4 and GFP-tagged pleckstrin homology (PH) domains (of design created by others: Szentpetery, Balla, Kim, Lemmon, & Balla, 2009). However, we do not recommend quantitative analyses with long-chain PIPs because they distribute non-uniformly into two populations of droplets, one of high PIP-concentration and one with no PIPs, presumably due to micellar formation in decane to shield the highly hydrophilic headgroups.

2.1 Materials

1. Hamilton 1000 series Gastight glass syringe with removable needle: 1 mL and 100 μL sizes, with 22-gauge needles (Hamilton, p/n 81365)
2. 2 mL glass vials with Teflon-lined caps (Thomas Scientific 1234R80)

Fig. 2 Dynamic and photoinducible protein interactions with membrane phospholipids in synthetic cell-like interfaces and eukaryotic cells. The positive control, BcLOV4, is recruited to membrane interfaces through a directly light-regulated electrostatic interaction with anionic phospholipids (see Glantz et al., 2018). Dissociation of photoactivated BcLOV4-mCherry from phospholipid interfaces in the dark is on similar biologically relevant timescales in vitro and in cellulo. (A) Exemplar fluorescence micrographs of BcLOV4 in droplets show that it is in the aqueous phase in the dark and is strongly recruited to the phospholipid-stabilized water/oil interface under blue light, only to revert to the water phase upon termination of illumination. Radial line profiles for time-lapse images taken before, during, and long after illumination may be used to quantitatively assess the ratio (R) of fluorescence signal at the boundary "b" to the interior "i." Scale bar = 20 μm. Blue light pulses: $\lambda = 440/20$ nm, 5 s, 15 mW/cm^2. mCherry imaging ($\lambda_{ex} = 550/15$ nm, $\lambda_{em} = 630/75$ nm). (B) Calculating the "R" ratio for droplets over time post-illumination reveals an exponentially decaying fluorescence intensity at the water/oil boundary and measurable dissociation kinetics, $\tau_{off} = 133$ s. (C) HEK cells. [i] Blue light-induced membrane recruitment (scale = 10 μm). [ii] Dissociation in the dark. (D) *S. cerevisiae* yeast. [i] Blue light-induced membrane recruitment (scale = 5 μm). [ii] Dissociation in the dark. All panels: 5 s. Blue light pre-illumination at irradiance = 15 mW/cm^2. *Panels c[i-ii] and d[i-ii]: From Glantz, S. T., Berlew, E. E., Jaber, Z., Schuster, B. S., Gardner, K. H., & Chow, B. Y. (2018). Directly light-regulated binding of RGS-LOV photoreceptors to anionic membrane phospholipids.* Proceedings of the National Academy of Sciences of the United States of America, 115*(33), E7720–E7727.*

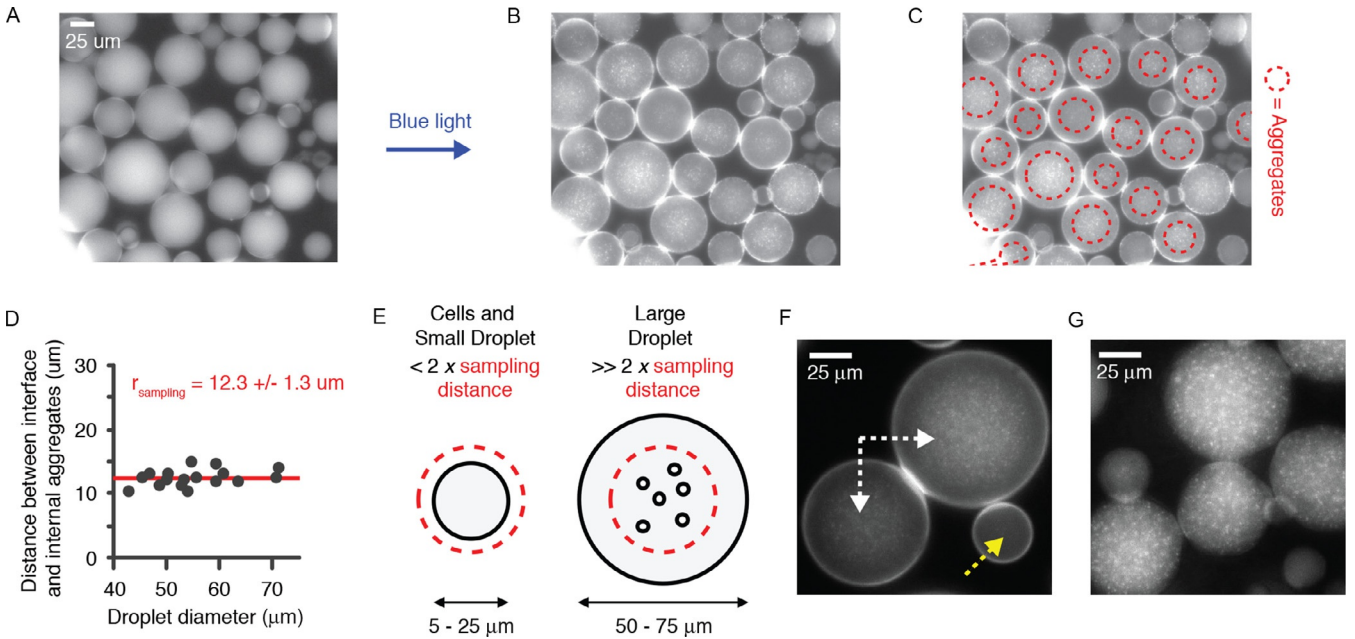

Fig. 3 Droplet-based high-content analysis of protein diffusional sampling distance. (A) Fluorescence micrograph showing BcLOV4-mCherry is uniformly distributed in the dark. (B) Upon illumination, BcLOV4 binds anionic phospholipid-stabilized interfaces when the membrane target is within the diffusional sampling distance of the protein, but forms colloidal protein aggregates in an electrostatically driven process at large distances from the interface because it is effectively in bulk solution unable to encounter its target. (C) In large droplets, the distance between the interface and the region of aggregates (highlighted in red) is consistent despite droplet size variation, with (D) a mean distance of 12.3 $\pm$ 1.3 μm as the empirically measured effective diffusional sampling distance. (E) Scheme of conditions under which BcLOV4 binds anionic membrane interfaces and/or self-aggregates. (F) Fluorescence micrograph of BcLOV4-mCherry bound nearly exclusively at the membrane interface in a small droplet (yellow arrow) devoid of aggregates, but with clear formation of aggregates in two large droplets (white arrows) as schematized in (E). (G) BcLOV4-mCherry aggregates form uniformly throughout 100% phosphotidylcholine droplets that lack negatively charged phospholipids at the water/oil interface.

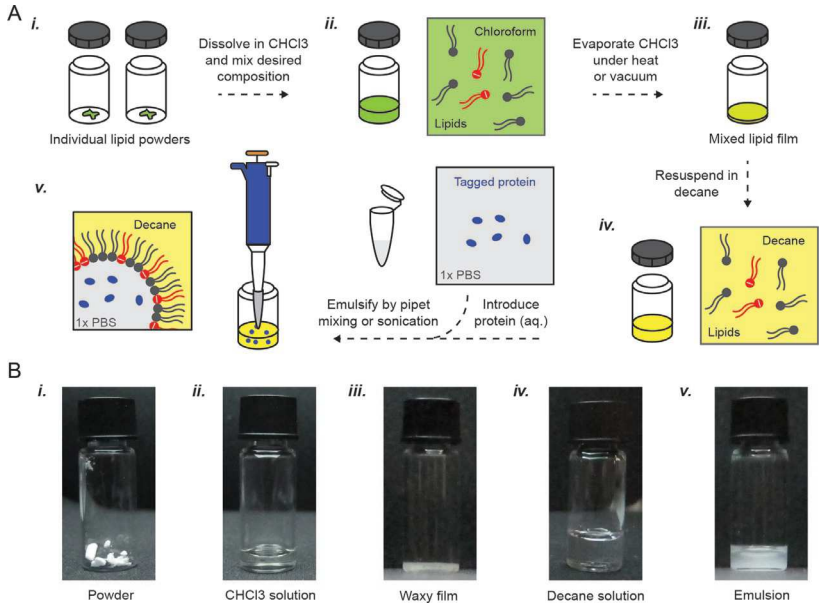

Fig. 4 Step-by-step preparation of the water-in-oil emulsions. (A) Schematic. See Supplementary File 1 in the online version at https://doi.org/10.1016/bs.mie.2019.02.015 for preparation volume calculator. (B) Optical images of 2 mL glass vials through the process, corresponding to the steps in (A) [i-v]. Note that multiple samples have been pooled for the turbid emulsion in image v. for increased volume for visual clarity.

3. Glass Pasteur pipette
4. Phospholipids of choice: e.g., phosphatidylcholine (PC; Avanti Polar Lipids 840051C), phosphatidylserine (PS; Sigma Aldrich P7769), phosphatidyl glycerol (PG; Sigma Aldrich, P8318), and phosphatidic acid (PA; Sigma Aldrich P9511)
5. Chloroform
6. Decane
7. Nitrogen/Argon gas, connected to a low-pressure airbrush or nitrogen spray gun
8. Fluorescently labeled candidate lipid-binding protein of interest (5–10 μM) in 1 × phosphate buffered saline (PBS)
9. Vacuum desiccator
10. Chemical fume hood
11. Water bath sonicator
12. Hotplate, preferably with sand or oil bath

2.2 Protocol

1. Using Hamilton syringes, prepare phospholipid stock solutions in chloroform:
   a. 32.6 m*M* PC (25 mg PC in 1 mL chloroform)
   b. 19 m*M* PS (15 mg PS in 1 mL chloroform)

Note 2.3. All work with chloroform and lipids should be performed in glass vials with Teflon-lined caps, and volume transfer should be performed with Hamilton syringes unless otherwise specified. Chloroform should be handled in a working fume hood.

2. Direct a stream of dry argon or nitrogen gas at the lipid solutions to evaporate the chloroform solvent. The chloroform should be gently agitated by the gas flow, and should not be splashing violently in the vial. When the organic solvent has been evaporated, a hazy lipid film should be visible at the bottom of the vial

Note 2.4. The glass vial will get very cold as the chloroform vaporizes. Throughout the vaporization process, rotating the vial in your gloved hand to warm it will increase the rate of evaporation and generate a more even lipid film on the bottom walls of the vial.

3. Completely dry the film of trace solvent by placing the vials in a vacuum desiccator chamber for 30 min at room temperature. Generally, "house vacuum" systems should be sufficient for this purpose

Note 2.5. Alternative to steps 2 and 3 above, the vial can be heated in a fume hood in a sand or oil bath, first at 40–50 °C to gently evaporate most the solvent, and then completely drying the film in vacuum or heating it above the chloroform boiling point (>62 °C).

4. Using Hamilton syringes, re-suspend the lipid film in decane. The following concentrations are appropriately soluble for PC and PS.
   c. 32.6 m*M* PC (25 mg PC in 1 mL decane)
   d. 19 m*M* PS (15 mg PS in 1 mL decane)
5. Solubilize the lipids in decane by water bath sonication for 2 min at room temperature. Then, heat the decane lipid stocks at 50 °C for 1–3 h. The stocks should be uniformly clear with no visible lipid films or clumps. These lipid stocks may be stored at −20 °C if not used immediately.
6. Blend phospholipids in decane to generate a desired lipid composition in the oil phase such that the total phospholipid concentration is 20 m*M* (see Supplementary File 1 in the online version at https://doi.org/10.1016/bs.mie.2019.02.015 for sample calculations for PC/PS droplets). Store the oil phase at −20 °C until ready for use.

7. Prepare the aqueous phase solution of fluorescently labeled protein in 1 × PBS (suggested protein concentration of 5–10 μ*M*).
8. Prepare water-in-oil emulsion droplets immediately prior to imaging them, by first transferring 30 μL of the lipid stock in decane to an Eppendorf tube.

Note 2.6. Steps 8–10 can be performed with adjustable non-glass pipettes. If the lipid stock has been previously frozen, warm the stock to at least room temperature to ensure accurate volume transfer of the viscous solutions in a pipette. Lipid-in-decane solutions can be heated to 37–42 °C if needed prior to handling.

9. Pipet 1.3 μL of the protein solution into the 30 μL decane mixture. The water phase should immediately sink to the bottom of the decane as a discrete aqueous phase.
10. Set a pipet to 20 μL volume. Place the pipet tip at the very bottom of the Eppendorf tube to access the aqueous phase and *gently* pipet up-and-down until the phase separation is noticeably disrupted. Then, pipet up-and-down vigorously (~30 s) until a uniformly cloudy suspension is visible (but, avoid foaming). This phospholipid-stabilized water-in-oil emulsion is ready for image analysis.

3. BcLOV4 control protein expression and purification

BcLOV4 (Glantz et al., 2018) is a versatile control protein with robust behavior in emulsion droplets. As a positive control, recruitment to net anionic interfaces is inducible with blue light (>15 mW/cm^2). Moreover, it can be made constitutively active in the dark as a non-inducible positive control with a single mutation that mimics the illuminated or active signaling state (Q355N) (Ganguly, Thiel, & Crane, 2017; Gleichmann, Diensthuber, & Möglich, 2013; Nash, Ko, Harper, & Gardner, 2008). In the presence of zwitterionic interfaces (e.g., 100% PC), the activated protein(s) will only self-aggregate in the absence of a suitably anionic membrane binding target. BcLOV4 can also serve as a negative control in the dark, or even in the presence of blue light by introducing a single mutation (C292A) that renders it photochemically inactive or unable to form the key photo-adduct (Christie, Swartz, Bogomolni, & Briggs, 2002) that drives the light-dependent protein-lipid interaction. In these cases, the protein should remain fairly monodisperse in the droplet interior.

The expression and affinity-purification of BcLOV4 largely follow standard research laboratory-scale protein production techniques for

His_6-tagged proteins, with a few notable exceptions. (i) The optically active protein should be shielded from short wavelength illumination to improve holoprotein yield. (ii) The imidazole concentration required to elute it is high/stringent to remove cleavage products of the multi-domain protein.

3.1 Materials

1. Aluminum foil
2. Absorbance spectrophotometer

3.1.1 Protein expression

3. BcLOV4-mCherry bacterial expression plasmids (Addgene IDs: wild-type [#114596]; constitutively active mutant Q355N [#119762]; photochemically incompetent mutant C292A [#119761])
4. BL21 (DE3) cells (NEB C2527H)
5. 37 °C shaking incubator, and refrigerated incubator with shaking
6. LB plate and LB media, both with 50 μg/mL kanamycin
7. 4 L baffled flask
8. isopropyl-beta-D-thiogalactopyranoside (IPTG)
9. Refrigerated centrifuge and 250 mL centrifuge bottles

3.1.2 Protein isolation

10. "cOmplete" mini EDTA-free protease inhibitor cocktail tables (Roche 04693159001)
11. Lysis buffer (50 m*M* NaP/500 m*M* NaCl/0.5% Triton X-100/pH 6.5/sterile-filtered)
12. 20 mL syringes and 21-gauge needles
13. Tip sonicator (≥60 W power)

3.1.3 Protein purification

14. FPLC with:
    i. 5 mL-volume NiNTA affinity resin column
    ii. wash buffer (50 m*M* NaP/500 m*M* NaCl/10% glycerol/pH 6.5/sterile-filtered)
    iii. elution buffer (50 m*M* NaP/500 m*M* NaCl/10% glycerol/500 m*M* imidazole/pH 6.5/sterile-filtered)
15. PD-10 desalting column with Sephadex G-25 resin

3.2 Protocol

3.2.1 Protein expression

1. Transform bacterial expression plasmid for BcLOV4-mCherry (kanamycin resistance marker) into BL21 (DE3) *Escherichia coli* cells by standard techniques (Sambrook, 2001) (also described in Glantz et al., 2018 for these particular plasmids), and plate onto LB plates with 50 μg/mL kanamycin.
2. Pick a single colony from the transformation plate, and grow cells to saturation ($OD_{600} \sim 2.0$) in 5 mL LB media with 50 μg/mL kanamycin overnight at 37 °C, with 250 rpm shaking.
3. To initiate the culture for protein production, dilute the saturated culture 1:200 into 1 L sterile LB-kanamycin media, in a 4 L baffled flask. Incubate the culture at 37 °C, 250 rpm, and measure its OD_{600} periodically until it reaches mid-log phase ($OD_{600} \sim 0.6$–0.8), which will typically take 4 h.
4. Induce protein production with 0.5 m*M* isopropyl-beta-D-thiogalactopyranoside (IPTG), and the transfer the culture to a dark refrigerated incubator at 18 °C, with 250 rpm shaking for 18–22 h. The window of the incubator should be covered to prevent light entry (e.g., aluminum foil) or filter blue light (e.g., amber/red acrylic).
5. Harvest the cells in 250 mL centrifuge bottles in a refrigerated centrifuge (5000 ×*g* for 25 min at 4 °C). Wrap the centrifuge bottles in aluminum foil to prevent light exposure, and then freeze the pellets at −20 °C for at least 1 h (and up to 2 weeks) prior to lysis and purification.

3.2.2 Protein isolation from cells

6. Thaw the frozen cells for 5–10 min at room temperature in the dark.
7. Dissolve two EDTA-free protease inhibitor tablets in 50 mL lysis buffer, and chill on ice.

Note 3.1. Carry out steps 8–11 on ice, or in a 4 °C cold room in the dark or under a red safelight illumination (e.g., photography darkroom LED bulbs).

8. Resuspend the thawed cells in the cold lysis buffer (50 mL per liter of harvested cell culture), by pipetting up-and-down with a 10 mL serological pipette.
9. Then, homogenize the suspended cells by passing them three times through a 20 mL syringe fitted with a 21-gauge needle.
10. Sonicate the lysate five times on ice with a duty cycle of 15 s on/30 s off, at ∼60 W power level. To ensure complete and thorough lysis, we recommend aliquoting the lysate into 10 mL fractions in 15 mL conical tubes and performing sonication on each fraction individually.

11. Pool the sonicated lysate into a 50 mL polycarbonate conical tube, and then clarify the solution by centrifugation (25,000 $\times g$ for 45 min at 4 °C). Decant the supernatant (i.e., clarified lysate) and store it on ice for further purification.

3.2.3 Protein purification

12. Purify the protein from the clarified lysate using fast protein liquid chromatography (FPLC). All non-opaque components of the FPLC that the sample can pass through should be covered with aluminum foil. Outfit the FPLC with a 5 mL Ni-NTA affinity purification column, wash buffer (designated line "A" here), and elution buffer (designated line "B" here).
13. Equilibrate the column with five column volumes of 4% buffer B. Load the clarified lysate onto the column at 1 mL/min, 4% B. Wash the column with 15 column volumes of 4% B.
14. Run a linear gradient from 4% to 40% B (20–200 m*M* imidazole) over 15 column volumes at 5 mL/min to wash truncated protein off the column. Then, elute BcLOV4-mCherry with 100% B (500 m*M* imidazole) and collect it in 10 × 2 mL fractions.
15. Assess sample purity by SDS-PAGE gel electrophoresis, and the protein concentration by absorbance spectroscopy (A280). Pool the most concentrated fractions.
16. Buffer-exchange 2.5 mL protein into 1 × PBS using a PD-10 desalting column. Centrifuge the eluted protein (25,000 $\times g$ at 4 °C for 30 min) to pellet insoluble protein.
17. Repeat step 16 twice more, re-equilibrating the desalting column with 25 mL 1 × PBS before each usage.
18. Determine the concentration of flavin-bound holoprotein by measuring A450, assuming a cofactor molar extinction coefficient of $\varepsilon = 12{,}500\ M^{-1}\ \mathrm{cm}^{-1}$.

4. Automated fluorescence imaging plates

Standard multi-well microplates for imaging are typically made from plastics like polystyrene that strongly bind phospholipids, leading to droplet instability and rapid accumulation at the microplate wall. However, plates made of acrylic and/or glass do not present such confounds. This section describes the fabrication of custom microwell plates that are defined by holes cut into an acrylic sheet, fused to cover glass as the plate bottom (Fig. 5).

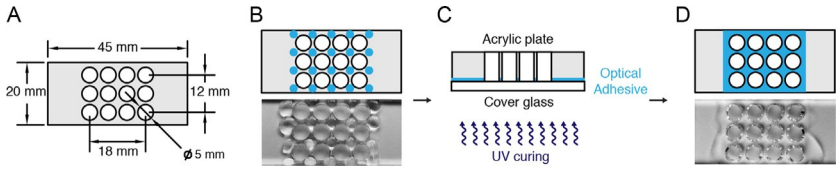

Fig. 5 Design and assembly of the imaging plate. An acrylic plate is required to avoid lipid interactions with the plastics of standard multiwell plate. (A) Dimensions of the acrylic cutout from the top down. (B) Top-down schematic and image of uncured optical adhesive droplet placement (drawn in blue), prior to placement of the coverglass. (C) Cross-sectional schematic of the imaging plate sandwich and optical adhesive curing process. (D) Top-down schematic and image of the cured imaging plate. The adhesive seals the crossroads of the grid, but should minimally seep into the circular wells so that imaging is entirely through the coverglass.

The 25 μL assay volume in the following section has been optimized for the microwell plate geometry described here in this section, resulting in a monolayer of droplets that are spaced with minimal overlap. However, this combination of microwell plate dimensions and sample volume is not prescribed, and alternative combinations are possible.

4.1 Materials

1. Laser cutter (or outsourced to machine shop)
2. $\geq 1/8''$-thick clear acrylic
3. Microscope cover glass, 25×25 mm, No. 1
4. Norland Optical Adhesive (#81)
5. UV lamp/LED

4.2 Protocol

1. Laser-cut plates from $>1/8''$ clear acrylic, with dimensions described in Fig. 5A. A CAD file is available in Supplementary File 2 in the online version at https://doi.org/10.1016/bs.mie.2019.02.015. To keep the piece clean, keep the adhesive paper-backing on when cutting, and cut the piece with the paper facing down on the stage.
2. Remove the paper backing from the acrylic plates
3. Apply a drop of Norland Optical Adhesive (#81) at each crossroad of the array of holes (dots as shown in Fig. 5B), using the applicator of the adhesive bottle. The adhesive droplets should be ~1 mm-diameter.
4. Cover the holes of the acrylic plate with the glass coverslip (one coverslip per acrylic plate) to form the bottom of the microwells. Ensure that a seal is formed around the circumference of each well, without excess adhesive oozing into the wells.

5. Cure the plates under a UV floodlight, with cover glass facing the light source. The duration will depend on the wavelength and irradiance of the light source; general guidelines and light source-specific protocols for curing are provided by the manufacturer.

Note 4.1. We use an IntelliRay 400 Shuttered UV Floodlight with Rayven curing chamber for 15 min ($\lambda = 365$ nm, irradiance $= 175\,\mathrm{mW/cm^2}$).

6. Store microwell plates in a clean and covered container to prevent dust accumulation.

5. Imaging dynamic membrane recruitment

For imaging analysis, droplets should be stable and not dynamically merge or coalesce into larger droplets. Monolayers of droplets spaced with minimal overlap provide suitably stable imaging conditions for most applications, with enough droplets per field-of-view for error analysis using 20–40× objective lenses. At 20×, 25–75 droplets should be in the field of view, with a mean droplet diameter ~20–50 μm.

The protocols below describe assays on an inverted epi-fluorescence microscope, which is suitable for screening and dynamic analyses on the timescale of a few minutes. However, if a confocal microscope is available, confocal microscopy is beneficial when imaging droplets that vary widely in diameter and thus have dissimilar midplanes across a single field-of-view, and also when imaging over extended time periods to account for droplet movement.

5.1 Materials

1. Inverted fluorescence microscope, equipped with automation software such as Micromanager or MetaMorph.
2. Additionally, for optogenetic induction with BcLOV4-mCherry, the microscope will require:
   a. Co-aligned and individually controlled LED light sources for BcLOV4 stimulation, (blue, $\lambda \sim 450$ nm) and mCherry imaging (yellow/amber, $\lambda \sim 570$ nm)
   b. Filter set that permits simultaneous imaging and optogenetic stimulation. For example: $\lambda > 585$ nm (long-pass) dichroic mirror, $\lambda = 630 \pm 37.5$ nm (bandpass) emission filter, with excitation wavelength controlled at the light source
3. Optical power meter
4. Microscope size standard

5.2 Protocols

5.2.1 General

1. Immediately prior to imaging, transfer 25–30 μL of freshly generated emulsion droplets to a new microwell.
2. Focus on the glass bottom of the microwell plate at 20 × magnification in brightfield mode, and raise the focal plane until droplets are clearly visible.
3. Use fine focus control to find the droplet top and bottom, and then, set the focus at the droplet midplane prior to fluorescence imaging.

5.2.2 Optical induction of the BcLOV4 control

4. Determine excitation source settings for BcLOV4 photo-stimulation with 15 mW/cm^2 blue light through a 20 × objective lens. Stimulation at this irradiance, which is the in vitro saturation value for BcLOV4, will limit cofactor photobleaching.
   a. Measure the beam power (in W or mW) with an optical power meter. The beam should be smaller than the detector area. If your power meter measures an irradiance (power/area), then multiply the reading by the detector area.
   b. Use a microscope size standard to determine the field-of-view of your objective lens (and approximate beam diameter), and then divide the measured power by this area.
5. Collect four mCherry fluorescence images, each separated by 15 s, to capture the "dark-state" images of the blue-light inducible system.
6. If only testing for droplet quality, skip this step and move on to step 7. To capture association dynamics, capture a 5 Hz-framerate movie with simultaneous excitation of BcLOV4 and mCherry.
7. Photo-stimulate BcLOV4 for 5 s with 15 mW/cm^2 blue light, and then image the mCherry tag. The protein should be membrane interface-localized. For determining undocking time constants by thermal reversion in the dark, image the droplets every 15 s for 5 min, without any further blue light-stimulation. An exponential fit should yield a time constant of ~0.5–2 min.

Note 5.1. Because of potential internal reflection at the interface of decane and water (and possibly the coverslip), which have different refractive indices, the degree of autofluorescence background under the imaging and concentration conditions should be assessed with the fluorescent protein or dye label alone.

6. Image analysis and segmentation

While the distribution of the protein within each droplet can be manually assessed (for example, using tools in ImageJ), such analysis becomes highly rate-limiting for the medium-to-high throughput assays possible. However, because the droplets are perfectly spherical such that they appear circular when imaged at their midplane, the individual droplets and their respective phase/compartment boundaries are easy to segment computationally. This section describes an automated analysis pipeline (Fig. 6) that finds circles of a given diameter range, and subsequently segments these circles further to distinguish the phospholipid boundary layer from the aqueous interior, and to quantify protein in each compartment. Note that some proteins are beyond a diffusional sampling distance from the membrane-like interface in large droplets ($\gg$25 μm diameter) and, thus, will not find the phospholipid monolayer accessible. Therefore, in this protocol, we have defined an interior "core" region for each droplet that eliminates any protein beyond the sampling distance from the interface.

Here, we provide code in MATLAB (Supplementary File 3 in the online version at https://doi.org/10.1016/bs.mie.2019.02.015) for analyzing BcLOV4, but the general approach described in the workflow of Fig. 6 and pseudocode in the protocol below should apply to other image analysis programs and proteins of interest.

6.1 Materials

1. Image analysis software (MATLAB)

6.2 Protocol (automated analysis workflow)

1. *Input file:* Stack of fluorescence micrographs showing the localization of a fluorescently tagged protein in emulsion droplets, with each image corresponding to a different timepoint.
2. Save the input image file as a variable name (in MATLAB, use "imread" function).
3. Identify the outermost boundary for all droplets with a given diameter range (in MATLAB, use "imfindcircles" function) and record each object's centroid coordinate and radius. This is the outer water/oil (w/o) interface boundary.

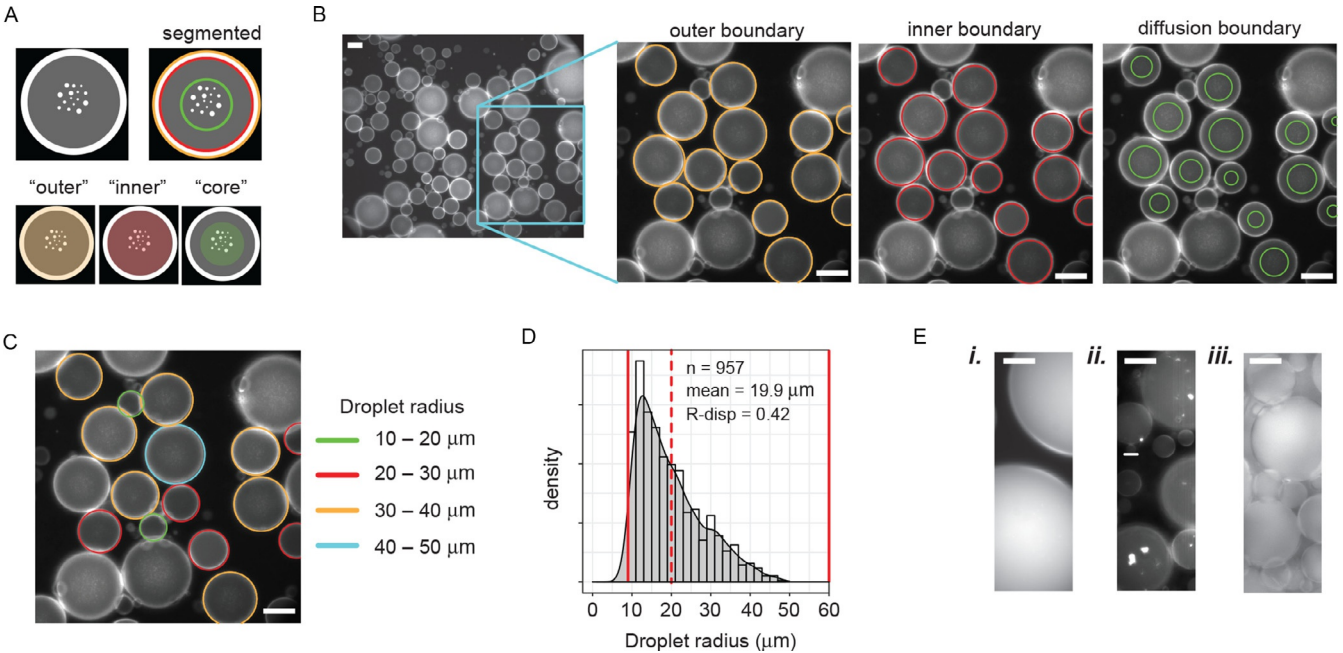

Fig. 6 Segmentation of the emulsion dispersed phase and droplet interface. (A) Schematic of a droplet with robust phospholipid-stabilized water/oil interface recruitment of activated BcLOV4 in the presence of negatively charged phospholipids, and internal aggregation beyond the diffusional sampling length from the droplet exterior. "Outer," "inner" and "core" masks are generated from boundary segmentation as described in the pseudocode. (B) Example MATLAB analysis of a fluorescence micrograph of phospholipid bound BcLOV4 in 80% PC/20% PS droplets in the illuminated state. Automated segmentation identifies the outer boundary (orange), the inner boundary (red) and the interior diffusional sampling length (green). (C) Droplets vary in radius where (D) the mean droplet radius is 19.9 μm (red dotted line) and the droplet R-dispersion is 0.42 for 957 droplets identified by MATLAB automated analysis that was set to find droplets ranging from 10 to 60 μm (solid red lines). (E) Common errors in droplet generation that compromise the segmentation and analysis include: [i] oversized droplets caused by poor emulsification due to insufficient vigor applied when by mixing by pipet. [ii] Internal protein aggregates from poor protein stability under the given buffer conditions. [iii] Difficult to resolve, overlapping droplets due to overloading of the microwell plate during imaging. (A-E) Scale bar = 50 μm.

Note 6.1. When finding circles, it is optimal to use a relatively narrow diameter range to improve detection speed and accuracy. Software programs will measure the circle diameter in pixels. Use a micron-scale size reference to convert image pixels to an experiment-relevant size range in microns. For example, at 3.14 pixels/μm, a 20–50 μm droplet diameter range corresponds to a diameter range of 63–157 pixels.

4. For each pair of outermost boundary radius and centroid, generate a virtual inner water/oil (w/o) interface boundary description by subtracting 3 μm in length from the radius.
5. For each pair of outermost boundary radius and centroid, generate a virtual dispersed phase diffusion boundary by subtracting the calculated diffusion length from the radius (for BcLOV4, 12 μm).
6. Generate three masks for each droplet: a mask that extends from the centroid to the (i) outermost boundary ("outer"), (ii) to the inner water/oil interface boundary ("inner"), and (iii) to the diffusion boundary ("core").
7. For each of the masked regions, calculate the area and sum the fluorescence intensity over all pixels.
8. Quantify the phospholipid boundary protein level as:

$$\text{Normalized boundary intensity} = \frac{\text{Intensity}\left(\text{“outer”} - \text{“inner”}\right)}{\text{Area}\left(\text{“outer”} - \text{“inner”}\right)}$$

9. Quantify the dispersed phase protein level as

$$\text{Normalized dispersed phase intensity} = \frac{\text{Intensity}\left(\text{“inner”} - \text{“core”}\right)}{\text{Area}\left(\text{“inner”} - \text{“core”}\right)}$$

10. To visualize the segmentation by image processing, draw circles on the image using the identified coordinates. In MATLAB, use "imshow" to display the original image and "viscircles" to display the found objects

Acknowledgments

We thank Jessica Bermudez, Matt Good, and Ben Schuster for helpful discussion in methods development. B.Y.C. acknowledges the support of National Science Foundation (NSF) Systems and Synthetic Biology (MCB 1652003), NSF Biophotonics (CBET 126497), NIH/National Institute on Drug Abuse (R21 DA040434), Penn Medicine Neuroscience

Center, W. W. Smith Charitable Trust for the Heart, NIH/National Institute of Neurological Disorders and Stroke (NINDS) (R01 NS101106). S.T.G. acknowledges the fellowship support of the NSF Graduate Research Fellowship Program and the Penn Center for Neuroengineering and Therapeutics Training Grant (NIH/NINDS; T32 NS091006).

References

Beseničar, M., Maček, P., Lakey, J. H., & Anderluh, G. (2006). Surface plasmon resonance in protein–membrane interactions. *Chemistry and Physics of Lipids*, *141*(1), 169–178.

Caldwell, R. M., Bermudez, J. G., Thai, D., Aonbangkhen, C., Schuster, B. S., Courtney, T., et al. (2018). Optochemical control of protein localization and activity within cell-like compartments. *Biochemistry*, *57*(18), 2590–2596.

Christie, J. M., Swartz, T. E., Bogomolni, R. A., & Briggs, W. R. (2002). Phototropin LOV domains exhibit distinct roles in regulating photoreceptor function. *The Plant Journal*, *32*(2), 205–219.

Dowler, S., Currie, R. A., Campbell, D. G., Deak, M., Kular, G., Downes, C. P., et al. (2000). Identification of pleckstrin-homology-domain-containing proteins with novel phosphoinositide-binding specificities. *The Biochemical Journal*, *351*(Pt. 1), 19–31.

Gallego, O., Betts, M. J., Gvozdenovic-Jeremic, J., Maeda, K., Matetzki, C., Aguilar-Gurrieri, C., et al. (2010). A systematic screen for protein–lipid interactions in *Saccharomyces cerevisiae*. *Molecular Systems Biology*, *6*(1), 430.

Ganguly, A., Thiel, W., & Crane, B. R. (2017). Glutamine amide flip elicits long distance allosteric responses in the LOV protein vivid. *Journal of the American Chemical Society*, *139*(8), 2972–2980.

Glantz, S. T., Berlew, E. E., Jaber, Z., Schuster, B. S., Gardner, K. H., & Chow, B. Y. (2018). Directly light-regulated binding of RGS-LOV photoreceptors to anionic membrane phospholipids. *Proceedings of the National Academy of Sciences of the United States of America*, *115*(33), E7720–E7727.

Gleichmann, T., Diensthuber, R. P., & Möglich, A. (2013). Charting the signal trajectory in a light-oxygen-voltage photoreceptor by random mutagenesis and covariance analysis. *Journal of Biological Chemistry*, *288*(41), 29345–29355.

Good, M. C. (2016). Encapsulation of Xenopus egg and embryo extract spindle assembly reactions in synthetic cell-like compartments with tunable size. *Methods in Molecular Biology*, *1413*, 87–108.

Good, M. C., Vahey, M. D., Skandarajah, A., Fletcher, D. A., & Heald, R. (2013). Cytoplasmic volume modulates spindle size during embryogenesis. *Science*, *342*(6160), 856–860.

Head, S. R., Komori, H. K., LaMere, S. A., Whisenant, T., Van Nieuwerburgh, F., Salomon, D. R., et al. (2014). Library construction for next-generation sequencing: Overviews and challenges. *BioTechniques*, *56*(2), 61–64.

Kavran, J. M., Klein, D. E., Lee, A., Falasca, M., Isakoff, S. J., Skolnik, E. Y., et al. (1998). Specificity and promiscuity in phosphoinositide binding by pleckstrin homology domains. *The Journal of Biological Chemistry*, *273*(46), 30497–30508.

Lauffenburger, D. A., & Linderman, J. (1993). *Receptors: Models for binding, trafficking, and signaling*. Oxford University Press.

Lee, S. H., Jin, J. B., Song, J., Min, M. K., Park, D. S., Kim, Y.-W., et al. (2002). The intermolecular interaction between the PH domain and the C-terminal domain of Arabidopsis dynamin-like 6 determines lipid binding specificity. *Journal of Biological Chemistry*, *277*(35), 31842–31849.

Liu, L., Li, Y., Li, S., Hu, N., He, Y., Pong, R., et al. (2012). Comparison of next-generation sequencing systems. *Journal of Biomedicine and Biotechnology*, *2012*, 11.

Lu, W.-C., & Ellington, A. D. (2013). In vitro selection of proteins via emulsion compartments. *Methods*, *60*(1), 75–80.

Lu, K.-Y., Tao, S.-C., Yang, T.-C., Ho, Y.-H., Lee, C.-H., Lin, C.-C., et al. (2012). Profiling lipid–protein interactions using nonquenched fluorescent liposomal nanovesicles and proteome microarrays. *Molecular & Cellular Proteomics*, *11*(11), 1177.

Narayan, K., & Lemmon, M. A. (2006). Determining selectivity of phosphoinositide-binding domains. *Methods*, *39*(2), 122–133.

Nash, A. I., Ko, W.-H., Harper, S. M., & Gardner, K. H. (2008). A conserved glutamine plays a central role in LOV domain signal transmission and its duration†. *Biochemistry*, *47*(52), 13842–13849.

Park, D., Tosello-Trampont, A.-C., Elliott, M. R., Lu, M., Haney, L. B., Ma, Z., et al. (2007). BAI1 is an engulfment receptor for apoptotic cells upstream of the ELMO/Dock180/Rac module. *Nature*, *450*, 430.

Pinheiro, L. B., Coleman, V. A., Hindson, C. M., Herrmann, J., Hindson, B. J., Bhat, S., et al. (2012). Evaluation of a droplet digital polymerase chain reaction format for DNA copy number quantification. *Analytical Chemistry*, *84*(2), 1003–1011.

Pykäläinen, A., Boczkowska, M., Zhao, H., Saarikangas, J., Rebowski, G., Jansen, M., et al. (2011). Pinkbar is an epithelial-specific BAR domain protein that generates planar membrane structures. *Nature Structural & Molecular Biology*, *18*, 902.

Sambrook, J. (2001). *Molecular cloning: A laboratory manual* (3rd ed.). . Cold Spring Harbor, NY: Cold Spring Harbor Laboratory Press.

Seelig, J. (2004). Thermodynamics of lipid–peptide interactions. *Biochimica et Biophysica Acta (BBA)—Biomembranes*, *1666*(1), 40–50.

Shao, K., Ding, W., Wang, F., Li, H., Ma, D., & Wang, H. (2011). Emulsion PCR: A high efficient way of PCR amplification of random DNA libraries in aptamer selection. *PLoS One*, *6*(9) e24910.

Szentpetery, Z., Balla, A., Kim, Y. J., Lemmon, M. A., & Balla, T. (2009). Live cell imaging with protein domains capable of recognizing phosphatidylinositol 4,5-bisphosphate; a comparative study. *BMC Cell Biology*, *10*(1), 67.

Tang, Y., Zeng, X., & Liang, J. (2010). Surface plasmon resonance: An introduction to a surface spectroscopy technique. *Journal of Chemical Education*, *87*(7), 742–746.

Tawfik, D. S., & Griffiths, A. D. (1998). Man-made cell-like compartments for molecular evolution. *Nature Biotechnology*, *16*(7), 652–656.

Tay, L. W. R., Wang, Z., & Du, G. (2017). Analysis of phosphatidic acid binding and regulation of PIPKI in vitro and in intact cells. In M. H. Gelb (Ed.), *Vol. 583. Methods in enzymology* (pp. 359–374). Academic Press.

Yu, J. W., Mendrola, J. M., Audhya, A., Singh, S., Keleti, D., DeWald, D. B., et al. (2004). Genome-wide analysis of membrane targeting by S. cerevisiae pleckstrin homology domains. *Molecular Cell*, *13*(5), 677–688.

Zhu, H., Bilgin, M., Bangham, R., Hall, D., Casamayor, A., Bertone, P., et al. (2001). Global analysis of protein activities using proteome chips. *Science*, *293*(5537), 2101.